

Fully Automatic Neural Network Reduction for Formal Verification

Tobias Ladner and Matthias Althoff

Abstract—Formal verification of neural networks is essential before their deployment in safety-critical applications. However, existing methods for formally verifying neural networks are not yet scalable enough to handle practical problems involving a large number of neurons. We address this challenge by introducing a fully automatic and sound reduction of neural networks using reachability analysis. The soundness ensures that the verification of the reduced network entails the verification of the original network. To the best of our knowledge, we present the first sound reduction approach that is applicable to neural networks with any type of element-wise activation function, such as ReLU, sigmoid, and tanh. The network reduction is computed on the fly while simultaneously verifying the original network and its specifications. All parameters are automatically tuned to minimize the network size without compromising verifiability. We further show the applicability of our approach to convolutional neural networks by explicitly exploiting similar neighboring pixels. Our evaluation shows that our approach can reduce the number of neurons to a fraction of the original number of neurons with minor outer-approximation and thus reduce the verification time to a similar degree.

Index Terms—Formal verification, neural networks, set-based computation, neural network reduction, sound abstraction.

I. INTRODUCTION

NEURAL networks achieve impressive results in a variety of fields, including natural language processing [1], computer vision [2], and medical imaging [3]. In recent years, neural networks have been deployed in safety-critical environments, such as human-robot interaction [4] and autonomous driving [5]. As real-life applications are inherently exposed to noise, such as measurement inaccuracies and external disturbances, the deployment of neural networks in safety-critical environments is limited due to their sensitivity to adversarial attacks [6]: Even small perturbations of the input to a neural network, which are often barely noticeable to the human eye, can lead to unexpected outputs, e.g., a different predicted classification of an image or a controller returning an unsafe action. Thus, the formal verification of neural networks has gained importance in recent years [7]–[9], where approaches rigorously prove that the output of neural networks meets given specifications.

A. Related Work

Early approaches [10], [11] focus on complete algorithms to verify neural networks with ReLU activations, where either the specifications are formally proven or a counterexample is extracted. However, it has been shown that verifying a neural

network with n ReLU activations is NP-hard [11]. Thus, computing its exact output set for a given input set requires solving up to 2^n linear subproblems. Recent developments are made towards incomplete algorithms, where the neural networks are abstracted to enclose the exact behavior of the network. These approaches often formulate the formal verification of neural networks as an optimization problem [11]–[14] or use reachability analysis [15]–[23].

Optimization-based verifiers reason about neural networks by introducing relaxed, linear constraints for the activation functions and solving these relaxed problems using linear programming, satisfiability modulo theories (SMT) solvers [11]–[14], or symbolic interval propagation [24]–[26]. Branch-and-bound strategies [27] can be beneficial by splitting the problem at the neuron level [28], [29], e.g., by splitting ReLU neurons into their linear parts. In general, algorithms that split the problem lead to an exponential time complexity [11], so that current state-of-the-art tools [8] use advanced branch-and-bound strategies [30]–[32] to verify neural networks.

Verifiers using reachability analysis propagate sets through the neural network and verify given specifications using the computed outer-approximative output set. Simple representatives of this approach use pure interval arithmetic [33] or convex set representations such as zonotopes [15], [16]. As with optimization-based verifiers, splitting the set can improve the results [34], [35]. Non-convex set representations are used to tightly enclose the output due to the inherent nonlinearity of neural networks, including Taylor models [17]–[19], [36], star sets [20], [21], [37], and polynomial zonotopes [22], [23], [38]. However, the scalability to state-of-the-art networks remains a major challenge for optimization-based approaches and approaches based on reachability analysis [8].

One promising research direction for improving the scalability is sound neural network reduction [39]–[42], taking advantage of the typical over-parametrization of neural networks [43]. Sound neural network reduction reduces the number of neurons and provides formal bounds for the maximum error due to this reduction to reason about the original network. This research direction is closely related to neural network compression [44], [45], where the main goal is to reduce memory usage and computation time, e.g., for deployment in embedded systems [45]. Examples of compression techniques are quantization [46] and pruning [47]. However, the lack of formal error bounds prevents applying these techniques to the formal verification of neural networks.

To the best of our knowledge, there exist only a few network reduction approaches with formal error bounds: An early approach categorizes neurons based on analytic properties and merges neurons of the same category afterward [39].

Tobias Ladner and Matthias Althoff are with the TUM School of Computation, Information, and Technology, Technical University of Munich, Germany (email: tobias.ladner@tum.de; althoff@tum.de).

This work is extended using interval neural networks [40], [42], [48], [49], where the weights of a neural network are replaced with intervals during the sound reduction. It is worth mentioning that the reduced network can be re-enlarged using residual reasoning [50]. For ReLU networks, it is also possible to merge neurons that are entirely in the nonpositive or nonnegative region, respectively, without inducing outer-approximations [51]. Network reductions can also be achieved by clustering similar neurons for inputs of a given dataset [41]; however, 80 – 90% of the neurons remain when formal error bounds are demanded. Most approaches only consider ReLU neurons, while [42], [49] also consider odd and monotone activation functions as tanh. We present a sound network reduction algorithm with formal error bounds for general element-wise activation functions.

B. Contributions

Our proposed approach reduces a neural network by merging similar neurons for given specifications. For example, consider a noisy image as an input set to a convolutional neural network. Neurons representing neighboring pixels often have similar values and thus can be merged during the verification process, which helps to reduce the size of the neural network. Such properties cannot be inferred when analyzing a neural network without considering a specific uncertain input. Our approach is orthogonal to many verification techniques, thus, they can be used as an underlying verification engine. We demonstrate our approach using reachability analysis with zonotopes [16], [52]. The extension to other set-based verification tools is straightforward, including Taylor models [18], [19], [36], star sets [20], [21], [37], and polynomial zonotopes [22], [23], [38]. The resulting reduced network can also be exported and verified using optimization-based verification tools. Our main contributions are summarized as follows:

- We present a novel, fully automatic approach to soundly reduce large neural networks by merging similar neurons for given specifications.
- The reduced network is constructed on the fly, and the verification of the reduced network entails the verification of the original network.
- Our approach is applicable to all neural networks with element-wise activation functions, including ReLU, sigmoid, and tanh.
- To the best of our knowledge, we present the first neural network reduction approach that explicitly considers convolutional neural networks.
- Although our approach requires computing a new reduced network for different specifications, we show applications where the reduced network can be successfully reused.
- We will publish our approach with the next release of CORA [53].

The remainder of this work is structured as follows: Sec. II introduces the notation and background for this work. Then, we present our novel, fully automatic, and sound network reduction approach in Sec. III. In Sec. IV, we discuss applications of our approach, including the reduction of convolutional neural networks and how the reduced network can be reused for

changed specifications. Finally, we evaluate our approach in Sec. V and draw conclusions in Sec. VI.

II. PRELIMINARIES

A. Notation

We denote scalars and vectors by lower-case letters, matrices by upper-case letters, and sets by calligraphic letters. The i -th element of a vector $v \in \mathbb{R}^n$ is written as $v_{(i)}$, and the element in the i -th row and j -th column of a matrix $A \in \mathbb{R}^{n \times m}$ is written as $A_{(i,j)}$. The i -th row and j -th column are written as $A_{(i,\cdot)}$ and $A_{(\cdot,j)}$, respectively. The concatenation of two matrices A and B is denoted by $[A \ B]$. For $n \in \mathbb{N}$, we denote the identity matrix by I_n , and we use the notation $[n] = \{1, \dots, n\}$. Let $\mathcal{C} \subseteq [n]$, then $A_{(\mathcal{C},\cdot)}$ extracts all rows $i \in \mathcal{C}$ in lexicographic order. We denote the cardinality of a discrete set \mathcal{C} by $|\mathcal{C}|$. Let $\mathcal{S} \subset \mathbb{R}^n$ be a continuous set, then $\mathcal{S}_{(i)}$ is its projection on the i -th dimension. The set-based evaluation of a function $f: \mathbb{R}^n \rightarrow \mathbb{R}^m$ is written as $f(\mathcal{S}) = \{f(x) \mid x \in \mathcal{S}\}$. Given two sets $\mathcal{S}_1, \mathcal{S}_2$, then the Minkowski sum is denoted by $\mathcal{S}_1 \oplus \mathcal{S}_2 = \{s_1 + s_2 \mid s_1 \in \mathcal{S}_1, s_2 \in \mathcal{S}_2\}$. The Cartesian product is written as $\mathcal{S}_1 \times \mathcal{S}_2 = \left\{ \begin{bmatrix} s_1^T & s_2^T \end{bmatrix}^T \mid s_1 \in \mathcal{S}_1, s_2 \in \mathcal{S}_2 \right\}$. An interval with bounds $l, u \in \mathbb{R}^n$, where $l \leq u$ holds element-wise, is denoted by $[l, u]$. We write \mathbb{R}_+ to refer to all positive real numbers.

B. Neural Networks

We first introduce feed-forward neural networks [54, Sec. 5.1] in their standard form and discuss the sound reduction of convolutional neural networks [54, Sec. 5.5.6] in Sec. IV-A.

Definition 1 (Layers of Neural Networks [54, Sec. 5.1]). *Let n_{k-1}, n_k denote the number of input and output neurons of a layer k . Further, let $W_k \in \mathbb{R}^{n_k \times n_{k-1}}, b_k \in \mathbb{R}^{n_k}$, and $\sigma_k(\cdot)$ be the respective continuous activation function (e.g., sigmoid and ReLU), which is applied element-wise. Then, the operation $L_k: \mathbb{R}^{n_{k-1}} \rightarrow \mathbb{R}^{n_k}$ for a given input $h_{k-1} \in \mathbb{R}^{n_{k-1}}$ is computed by*

$$L_k(h_{k-1}) = \begin{cases} W_k h_{k-1} + b_k & \text{if layer } k \text{ is linear,} \\ \sigma_k(h_{k-1}) & \text{otherwise.} \end{cases}$$

Definition 2 (Neural Networks [54, Sec. 5.1]). *Given κ alternating linear and nonlinear layers, n_0 input and n_κ output neurons, let $x \in \mathbb{R}^{n_0}$ be the input and $y \in \mathbb{R}^{n_\kappa}$ be the output of a neural network, we can formulate a neural network Φ with $y = \Phi(x)$ as follows:*

$$\begin{aligned} h_0 &= x, \\ h_k &= L_k(h_{k-1}), \quad k \in [\kappa], \\ y &= h_\kappa. \end{aligned}$$

The last linear and last nonlinear layers are called output layers, all other layers are called hidden layers. If all hidden layers output the same number of neurons, we write 6×200 to refer to a network with 6 linear and 6 nonlinear hidden layers with 200 neurons each.

C. Set-Based Computing

We use sets for the formal verification of neural networks. Let $\mathcal{X} \subset \mathbb{R}^{n_0}$ be the input set of a neural network Φ . Then, the exact output set $\mathcal{Y}^* = \Phi(\mathcal{X})$ is computed by

$$\begin{aligned} \mathcal{H}_0^* &= \mathcal{X}, \\ \mathcal{H}_k^* &= L_k(\mathcal{H}_{k-1}^*), \quad k \in [\kappa], \\ \mathcal{Y}^* &= \mathcal{H}_\kappa^*. \end{aligned} \quad (1)$$

Our reduction approach works for any set representation that can be enclosed by an interval and that are closed under the Minkowski addition of intervals. We use zonotopes as an example to demonstrate our approach:

Definition 3 (Zonotope [52, Def. 1]). *Given a center vector $c \in \mathbb{R}^n$ and a generator matrix $G \in \mathbb{R}^{n \times q}$, a zonotope is defined as*

$$\mathcal{Z} = \langle c, G \rangle_{\mathcal{Z}} = \left\{ c + \sum_{j=1}^q \beta_j G_{(\cdot, j)} \mid \beta_j \in [-1, 1] \right\}.$$

For zonotopes, the required operations are computed as follows:

Proposition 1 (Interval Enclosure [55, Prop. 2.2]). *Given a zonotope $\mathcal{Z} = \langle c, G \rangle_{\mathcal{Z}}$, the enclosing interval $[l, u] = \text{interval}(\mathcal{Z}) \supseteq \mathcal{Z}$ is*

$$\begin{aligned} l &= c - \Delta g, \\ u &= c + \Delta g, \end{aligned} \quad \text{with } \Delta g = \sum_{j=1}^q |G_{(\cdot, j)}|.$$

Proposition 2 (Interval Addition [55, Eq. 2.1]). *Given a zonotope $\mathcal{Z} = \langle c, G \rangle_{\mathcal{Z}} \subset \mathbb{R}^n$ and an interval $\mathcal{I} = [l, u] \subset \mathbb{R}^n$,*

$$\mathcal{Z} \oplus \mathcal{I} = \langle c + c_{\mathcal{I}}, [G \text{diag}(u - c_{\mathcal{I}})] \rangle_{\mathcal{Z}},$$

where $c_{\mathcal{I}} = \frac{l+u}{2}$ and $\text{diag}(\cdot)$ returns a diagonal matrix.

D. Neural Network Verification

We briefly introduce the main steps to propagate a zonotope through a neural network. Since the propagation in (1) cannot be computed exactly in general, we enclose the output of each layer:

Proposition 3 (Image Enclosure [16, Sec. 3]). *Let $\mathcal{H}_{k-1} \supseteq \mathcal{H}_{k-1}^*$ be an input set to layer k , then*

$$\mathcal{H}_k = \text{enclose}(L_k, \mathcal{H}_{k-1}) \supseteq \mathcal{H}_k^*$$

computes an outer-approximative output set.

While zonotopes can be propagated through linear layers exactly [52], the propagation through nonlinear layers has to be outer-approximative to ensure soundness. The main steps to enclose the output of nonlinear layers are illustrated in Fig. 1: For each nonlinear layer, we iterate over all neurons i in the current layer by projecting the input set \mathcal{H}_{k-1} onto its i -th dimension (Step 1) and determining the input bounds using Prop. 1 (Step 2). We then find an approximating linear function within the input bounds via regression [54, Sec. 3] (Step 3). A key challenge is bounding the approximation error (Step 4): For piecewise linear activation functions, e.g. ReLU, we can

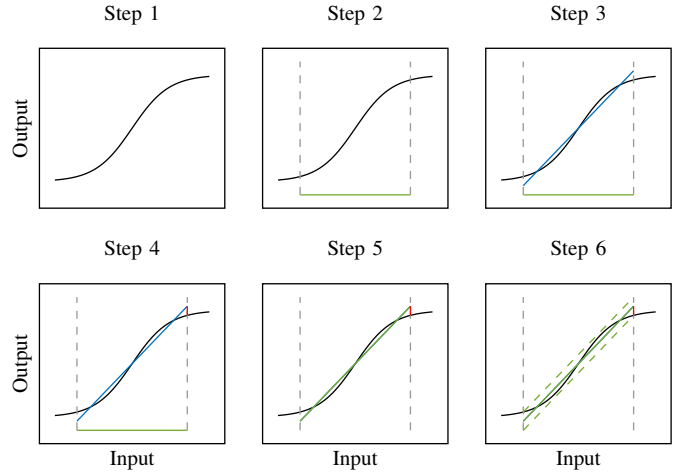


Fig. 1. Main steps of enclosing a nonlinear layer. Step 1: Neuron-wise sigmoid function. Step 2: Input bounds. Step 3: Approximating linear function. Step 4: Approximation error. Step 5: Apply linear transformation on input. Step 6: Enclose using approximation error.

compute the approximation error exactly using the extreme points of the difference between the approximation polynomial and each linear segment. For other activation functions, e.g. sigmoid, the approximation error can be determined by an analytic solution for specific polynomials, or sampling evenly within the input bounds and bounding the approximation error between two points via global bounds of the derivative [22, Sec. 3]. Finally, we apply the linear transformation on $\mathcal{H}_{k-1(i)}$ to approximate the nonlinear layer (Step 5) and enclose the activation function using the approximation error (Step 6; Prop. 2). Thus, by propagating a given input set \mathcal{X} through all layers of a neural network and enclosing their output sets using Prop. 3, we can enclose the exact output set by $\mathcal{Y} = \mathcal{H}_\kappa \supseteq \mathcal{Y}^* = \Phi(\mathcal{X})$.

E. Problem Statement

Given an input set $\mathcal{X} \subset \mathbb{R}^{n_0}$, a neural network Φ , and an unsafe set $\mathcal{S} \subset \mathbb{R}^{n_\kappa}$, we want to automatically construct a sound reduced network $\hat{\Phi}$, for which the verification entails the verification of the original network for the given \mathcal{X} and \mathcal{S} :

$$\hat{\Phi}(\mathcal{X}) \cap \mathcal{S} = \emptyset \implies \Phi(\mathcal{X}) \cap \mathcal{S} = \emptyset. \quad (2)$$

III. AUTOMATIC NEURAL NETWORK REDUCTION

Our sound neural network reduction is based on the observation that many neurons in a layer k behave similarly for a specific input $x \in \mathbb{R}^{n_0}$, e.g., many sigmoid neurons are fully saturated and thus output a value near 1 as shown in Fig. 2. Neuron saturation [56] and neural activation patterns [57] have been observed in the literature, however, to the best of our knowledge, they have not been exploited for the verification of neural networks. Our main idea is to merge these saturated neurons and provide the corresponding error bounds for an uncertain input $\mathcal{X} \subset \mathbb{R}^{n_0}$ (Fig. 3). Please note that our approach is not restricted to the saturation values of an activation function.

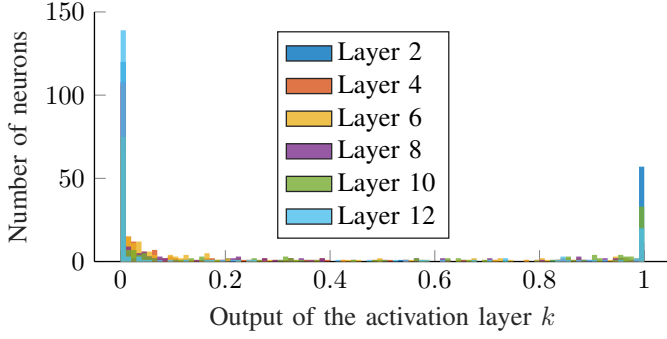


Fig. 2. Sigmoid activations of a 6×200 neural network with an image input from the MNIST digit dataset. For a specific input x , many neurons output values close to the saturation values 0 and 1.

A. Neuron Merging

Subsequently, we explain how similar neurons can help to construct a reduced network $\hat{\Phi}$, where the verification of $\hat{\Phi}$ entails the verification of the original network Φ . We gather the neurons with similar values using merge buckets (Fig. 3):

Definition 4 (Merge Buckets). *Given output bounds $\mathcal{I}_k \supseteq \mathcal{H}_k^*$ of a nonlinear layer $k \in [\kappa]$ with n_k neurons, an output $y \in \mathbb{R}$, and a tolerance $\delta \in \mathbb{R}_+$, then a merge bucket is defined as*

$$\mathcal{B}_{k,y,\delta} = \{i \in [n_k] \mid \mathcal{I}_{k(i)} \subseteq [y - \delta, y + \delta]\}.$$

Conceptually, we replace all neurons in a merge bucket $\mathcal{B}_{k,y,\delta}$ by a single neuron w' with constant output y and adjust the weight matrices of the linear layers $k-1$ and $k+1$ such that the reduced network $\hat{\Phi}$ approximates the behavior of the original network Φ . Finally, we add an approximation error to the output to obtain a sound outer-approximation (Fig. 3).

Proposition 4 (Neuron Merging). *Given a nonlinear hidden layer $k \in [\kappa]$ of a network Φ , output bounds $\mathcal{I}_k \supseteq \mathcal{H}_k^*$, a merge bucket \mathcal{B} , and the indices of the remaining neurons $\bar{\mathcal{B}} = [n_k] \setminus \mathcal{B}$, we can construct a sound reduced network $\hat{\Phi}$, where we remove the merged neurons by adjusting the linear layers $k-1$, $k+1$, and \hat{b}_{k+1} includes the approximation error:*

$$\begin{aligned} \widehat{W}_{k-1} &= W_{k-1(\bar{\mathcal{B}}, \cdot)}, & \widehat{b}_{k-1} &= b_{k-1(\bar{\mathcal{B}})}, \\ \widehat{W}_{k+1} &= W_{k+1(\cdot, \bar{\mathcal{B}})}, & \widehat{b}_{k+1} &= b_{k+1} \oplus \underbrace{W_{k+1(\cdot, \mathcal{B})} \mathcal{I}_k(\mathcal{B})}_{\text{approximation error}}. \end{aligned}$$

We denote the layer operations of the reduced network $\hat{\Phi}$ with \widehat{L}_k . The construction is sound.

Proof. Soundness. We show that the output $\widehat{\mathcal{H}}_{k+1}$ of layer $k+1$ of the reduced network $\hat{\Phi}$ is an outer-approximation of the exact set \mathcal{H}_{k+1}^* :

$$\begin{aligned} \mathcal{H}_{k+1}^* &\stackrel{(1)}{=} L_{k+1} \left(L_k \left(L_{k-1}(\mathcal{H}_{k-2}^*) \right) \right) \\ &\stackrel{(\text{Def. 1})}{=} L_{k+1} \left(L_k \left(W_{k-1}(\mathcal{H}_{k-2}^*) + b_{k-1} \right) \right). \end{aligned}$$

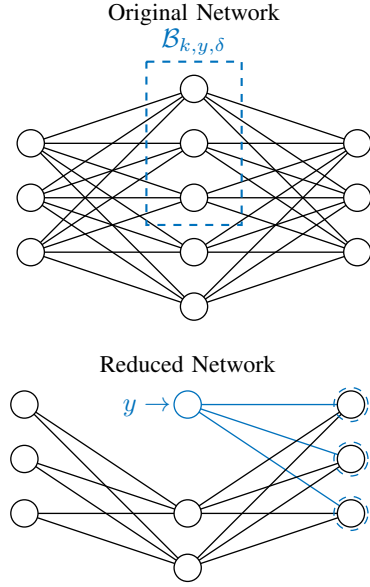


Fig. 3. Neural network reduction example using a single merge bucket $\mathcal{B}_{k,y,\delta}$: All neurons within $\mathcal{B}_{k,y,\delta}$ get replaced by a single neuron with output y (in blue). An approximation error is added to the subsequent neurons.

Without loss of generality, we relabel the neurons such that $\mathcal{B} := [|\mathcal{B}|]$ and partition the neurons of layer k accordingly:

$$\begin{aligned} \mathcal{H}_{k+1}^* &= L_{k+1} \left(L_k \left(\left(W_{k-1(\mathcal{B}, \cdot)} \mathcal{H}_{k-2}^* + b_{k-1(\mathcal{B})} \right) \right. \right. \\ &\quad \left. \left. \times \left(W_{k-1(\bar{\mathcal{B}}, \cdot)} \mathcal{H}_{k-2}^* + b_{k-1(\bar{\mathcal{B}})} \right) \right) \right) \\ &\stackrel{(\text{Def. 1})}{=} L_{k+1} \left(L_k \left(\mathcal{H}_{k-1(\mathcal{B})}^* \right) \times \widehat{L}_k \left(\widehat{L}_{k-1}(\mathcal{H}_{k-2}^*) \right) \right). \end{aligned}$$

We then enclose all merged neurons by the given interval bounds:

$$\mathcal{H}_{k+1}^* \stackrel{(\text{Def. 4})}{\subseteq} L_{k+1} \left(\mathcal{I}_k(\mathcal{B}) \times \widehat{L}_k \left(\widehat{L}_{k-1}(\mathcal{H}_{k-2}^*) \right) \right) = \mathcal{H}'_{k+1},$$

and propagate them forward to the next nonlinear layer $k+1$. This operation implicitly propagates the new constant neuron forward to the bias of the layer $k+1$ as well without inducing additional outer-approximations. Thus, using the identity $W(\tilde{\mathcal{I}}_1 \times \tilde{\mathcal{I}}_2) = W_{(\cdot, \mathcal{B})} \tilde{\mathcal{I}}_1 \oplus W_{(\cdot, \bar{\mathcal{B}})} \tilde{\mathcal{I}}_2$, we obtain:

$$\begin{aligned} \mathcal{H}'_{k+1} &\stackrel{(\text{Def. 1})}{=} W_{k+1} \left(\mathcal{I}_k(\mathcal{B}) \times \widehat{L}_k \left(\widehat{L}_{k-1}(\mathcal{H}_{k-2}^*) \right) \right) + b_{k+1} \\ &= \left(W_{k+1(\cdot, \mathcal{B})} \mathcal{I}_k(\mathcal{B}) \oplus W_{k+1(\cdot, \bar{\mathcal{B}})} \widehat{L}_k \left(\widehat{L}_{k-1}(\mathcal{H}_{k-2}^*) \right) \right) \\ &\quad + b_{k+1}. \end{aligned}$$

Finally, rearranging the terms and enclosing the output of all reduced layers using Prop. 3 obtains:

$$\begin{aligned} \mathcal{H}'_{k+1} &= W_{k+1(\cdot, \bar{\mathcal{B}})} \widehat{L}_k \left(\widehat{L}_{k-1}(\mathcal{H}_{k-2}^*) \right) \\ &\quad \oplus (b_{k+1} + W_{k+1(\cdot, \mathcal{B})} \mathcal{I}_k(\mathcal{B})) \\ &= \widehat{L}_{k+1} \left(\widehat{L}_k \left(\widehat{L}_{k-1}(\mathcal{H}_{k-2}^*) \right) \right) \stackrel{(\text{Prop. 3})}{\subseteq} \widehat{\mathcal{H}}_{k+1}, \end{aligned}$$

which shows that $\mathcal{H}_{k+1}^* \subseteq \mathcal{H}'_{k+1} \subseteq \widehat{\mathcal{H}}_{k+1}$. \square

B. Initialization of Merge Buckets

By iteratively applying Prop. 4, our approach can be naturally extended to multiple disjoint merge buckets:

$$\mathcal{B}_{k,\delta} = \{\mathcal{B}_{k,y_1,\delta}, \mathcal{B}_{k,y_2,\delta}, \dots\}. \quad (3)$$

The merging with multiple disjoint merge buckets can be done in parallel as the required adaptations of the adjacent linear layers do not interfere with each other. The overall approximation error is then given by the Minkowski sum of the individual approximation errors (Prop. 4):

$$\bigoplus_{\mathcal{B} \in \mathcal{B}} W_{k+1}(\cdot, \mathcal{B}) \mathcal{I}_k(\mathcal{B}) = W_{k+1}(\cdot, \bigcup_{\mathcal{B} \in \mathcal{B}} \mathcal{B}) \mathcal{I}_k(\bigcup_{\mathcal{B} \in \mathcal{B}} \mathcal{B}). \quad (4)$$

We define two different methods to initialize merge buckets.

a) *Static buckets*: The merge buckets are determined by the asymptotic values of the respective activation function σ_k of a nonlinear layer k :

$$\mathcal{B}_{k,\delta} = \begin{cases} \{\mathcal{B}_{k,0,\delta}, \mathcal{B}_{k,1,\delta}\} & \text{if } \sigma_k(x) = \text{sigmoid}(x), \\ \{\mathcal{B}_{k,-1,\delta}, \mathcal{B}_{k,1,\delta}\} & \text{if } \sigma_k(x) = \tanh(x), \\ \{\mathcal{B}_{k,0,\delta}\} & \text{if } \sigma_k(x) = \text{ReLU}(x). \end{cases} \quad (5)$$

For ReLU layers, setting $\delta = 0$ and using static merge buckets results in no approximation error similar to the approach in [51], as only neurons with entirely negative input for the given input set \mathcal{X} are removed.

b) *Dynamic buckets*: The merge buckets are dynamically initialized using the center of the bounds $\mathcal{I}_k = [l_k, u_k] \subset \mathbb{R}^{n_k}$ of each neuron:

$$\mathcal{B}_{k,\delta} = \{\mathcal{B}_{k,c(i),\delta} \mid c = \frac{l_k + u_k}{2}, i \in [n_k]\}, \quad (6)$$

where we ensure that the buckets are disjoint and are only used if they contain multiple neurons. Please note that the buckets could also be created using clustering algorithms similar to the approach in [41]; however, we choose the center of each neuron directly to obtain a linear computational overhead. The computational overhead of clustering algorithms might be negligible for other underlying verification engines than the zonotope approach considered in this work.

C. Automatic Determination of Bucket Tolerances

The bucket tolerance $\delta \in \mathbb{R}_+$ influences how many neurons are merged, where a larger value results in more aggressive neuron merging and thus a larger outer-approximation. However, determining a good value for δ is tedious as it is not immediately clear how much the network is reduced for any given value for δ . Thus, we automatically determine δ given the desired remaining number of neurons in Alg. 1 using a binary search algorithm. We denote the ratio of remaining neurons compared to the original network with the reduction rate $\rho \in [0, 1]$. To verify given specifications, we initially choose a very small ρ and iteratively increase it if the reduction is too outer-approximative. This realizes us to verify many specifications using a heavily reduced network (Sec. V), and thus to a similar degree the verification time is reduced. Once $\rho = 1$ is reached, the original network is used and no reduction is applied.

Algorithm 1 Automatic Determination of Bucket Tolerance

Require: Bounds \mathcal{I}_k , reduction rate ρ

```

1:  $\delta_{\min} \leftarrow 0, \delta_{\max} \leftarrow 0.01$ 
2: do ▷ Find upper bound for bucket tolerance
3:    $\delta_{\max} \leftarrow 10 * \delta_{\max}$ 
4:   Initialize merge buckets  $\mathcal{B}_{k,\delta_{\max}}$  ▷ Sec. III-B
5:    $\hat{n}_k \leftarrow n_k - \sum_{\mathcal{B} \in \mathcal{B}_{k,\delta_{\max}}} |\mathcal{B}|$  ▷ Remaining neurons
6:   while  $\hat{n}_k/n_k > \rho$ 
7:   do ▷ Binary search
8:      $\delta \leftarrow (\delta_{\min} + \delta_{\max})/2$ 
9:     Initialize merge buckets  $\mathcal{B}_{k,\delta}$  ▷ Sec. III-B
10:     $\hat{n}_k \leftarrow n_k - \sum_{\mathcal{B} \in \mathcal{B}_{k,\delta}} |\mathcal{B}|$  ▷ Remaining neurons
11:    if  $\hat{n}_k < \rho n_k$  then
12:       $\delta_{\max} \leftarrow \delta$  ▷ Too many neurons merged
13:    else
14:       $\delta_{\min} \leftarrow \delta$  ▷ Too few neurons merged
15:    end if
16:  while  $\hat{n}_k/n_k \not\approx \rho$ 
17:  return  $\mathcal{B}_{k,\delta}$ 

```

D. On-the-fly Neural Network Reduction

We require output bounds \mathcal{I}_k of the next nonlinear layer k to merge neurons with similar values using Prop. 4. However, computing them requires the construction of high-dimensional zonotopes via the linear layer $k - 1$ and the propagation of the zonotopes through the nonlinear layer k , where we have to compute the image enclosure for all neurons (Prop. 3) – which is what should be avoided. Thus, we deploy a one-step look-ahead algorithm (Alg. 2) using interval arithmetic [58] to avoid these expensive computations and reduce the network on the fly. As the look-ahead is just a single step, the computed bounds are tight and do not contribute to the wrapping effect.

We summarize Alg. 2 subsequently: Instead of propagating the zonotope itself forward, we just propagate interval bounds of \mathcal{H}_{k-2} to the next nonlinear layer k (line 4-5). Although intervals are not closed under the linear map, the output bounds of the linear layer $k - 1$ are tight and the propagation

Algorithm 2 On-the-fly Neural Network Reduction

Require: Input \mathcal{X} , neural network layers $L_k, k \in [\kappa]$,

```

reduction rate  $\rho$ 
1:  $\mathcal{H}_0 \leftarrow \mathcal{X}, \hat{L}_1 \leftarrow L_1$ 
2: for  $k = 2, 4, \dots, \kappa$  do
3:   if  $k < \kappa$  then ▷ 1) Look ahead
4:      $\mathcal{I}_{k-2} \leftarrow \text{interval}(H_{k-2})$  ▷ Prop. 1
5:      $\mathcal{I}_k \leftarrow L_k(\hat{L}_{k-1}(\mathcal{I}_{k-2}))$ 
6:     Determine merge buckets  $\mathcal{B}_{k,\delta}$  ▷ Sec. III-C
7:      $\hat{L}_{k-1}, \hat{L}_k, \hat{L}_{k+1} \leftarrow \text{Merge neurons}$  ▷ Prop. 4
8:   end if
9:   ▷ 2) Verify reduced network
10:   $\mathcal{H}_{k-1} \leftarrow \text{enclose}(\hat{L}_{k-1}, \mathcal{H}_{k-2})$  ▷ Prop. 3
11:   $\mathcal{H}_k \leftarrow \text{enclose}(\hat{L}_k, \mathcal{H}_{k-1})$ 
12: end for
13: return  $\mathcal{Y} \leftarrow \mathcal{H}_\kappa$ 

```

through the nonlinear layer k does not induce additional outer-approximations. This realizes a tight computation of the output bounds \mathcal{I}_k with negligible computational overhead. After \mathcal{I}_k is obtained, the merge buckets are determined (line 6) and the network is reduced by merging the respective neurons (line 7). Finally, we propagate the zonotope \mathcal{H}_{k-2} through the reduced layers. Thus, we never construct a high-dimensional zonotope during the verification. Note that the number of input and output neurons remains unchanged.

Theorem 1 (Sound Network Reduction). *Given an input set \mathcal{X} , a neural network Φ , and a reduction rate ρ , Alg. 2 constructs a reduced network $\hat{\Phi}_\rho$ satisfying the problem statement in Sec. II-E.*

Proof. The algorithm is sound as each step is outer-approximative. \square

IV. APPLICATIONS

In this section, we discuss applications of our novel neural network reduction approach and evaluate them in Sec. V.

A. Reduction of Convolutional Neural Networks

Convolutional neural networks are obtaining state-of-the-art results for image classification tasks [2]. However, neural networks for image classification are typically very large and thus particularly hard to verify. We show in this section that our novel neural network reduction approach can be naturally extended to convolutional networks. Let us start by introducing the main layer within a convolutional network:

Definition 5 (Convolutional Layer [54, Sec. 5.5.6]). *Given an input $I \in \mathbb{R}^{c_I \times h_I \times w_I}$ and a kernel $K \in \mathbb{R}^{c_O \times c_I \times h_K \times w_K}$, a convolutional layer computes the output $O \in \mathbb{R}^{c_O \times h_O \times w_O}$ for $k \in [c_O]$, $i \in [h_O]$, $j \in [w_O]$ as follows:*

$$O_{(k,i,j)} = \sum_{l=1}^{c_I} \sum_{m=1}^{h_K} \sum_{n=1}^{w_K} K_{(k,l,m,n)} I_{(l,i+m,j+n)},$$

where $h_O = h_I - (h_K - 1)$, $w_O = w_I - (w_K - 1)$ and c_I, c_O are the number of input and output channels, respectively.

Convolutional layers can be viewed as linear layers as defined in Def. 1 with shared weights [54, Sec. 5.5.6]. Thus, the same operation as in Def. 5 can be computed by flattening the input image I into a vector:

$$\vec{I} = [I_1 \ \dots \ I_{c_I}]^T, \quad (7)$$

with $I_l = [I_{(l,1,\cdot)} \ \dots \ I_{(l,h_I,\cdot)}]$, $l \in [c_I]$,

and correctly populating each row of the sparse weight matrix $W_K \in \mathbb{R}^{(c_O \cdot h_O \cdot w_O) \times (c_I \cdot h_I \cdot w_I)}$ with the kernel K :

$$W_K = \begin{bmatrix} K_{(1,1,1,1)} & K_{(1,1,1,2)} & \dots & 0 \\ 0 & K_{(1,1,1,1)} & \ddots & 0 \\ \vdots & \ddots & \ddots & \vdots \\ 0 & \dots & \dots & K_{(c_O,c_I,h_K,w_K)} \end{bmatrix}. \quad (8)$$

An analogous conversion can be done for other typical layers within a convolutional network, such as subsampling and average pooling layers [54, Sec. 5.5.6].

One important property of convolutional networks is the preservation of neighborhood: As the same kernel is applied to the entire input, pixels of the output have similar values if the respective pixels in the input have similar values. Neighboring pixels having similar values are typical in the field of image classification because many images contain large areas or objects with a similar color. For example, the sky has similar shades of blue, and traffic signs typically have only one background color and one foreground color. It is thus important to use dynamic merge buckets (Sec. III-B) as these colors might not be at the saturation points of the activation function. To the best of our knowledge, our approach is the first to explicitly exploit this property of convolutional networks for sound neural network reduction.

Intuitively, an uncertain image is compressed into superpixels with formal error bounds. Let us demonstrate this by an example: CIFAR-10 images require $32 \times 32 \times 3 = 3072$ input neurons to the network. However, many of these pixels have very similar values (Fig. 4). Thus, using our approach with dynamic merge buckets, we can compress an image as follows:

Corollary 1 (Sound Compression). *Given an uncertain image $\mathcal{X} \subset \mathbb{R}_+^{c_I \times h_I \times w_I}$ and a reduction rate $\rho \in [0, 1]$, we can construct a neural network $\hat{\Phi}_\rho$ that compresses this image with formal error bounds as follows: Let $K \in \mathbb{R}^{3 \times 3 \times 1 \times 1}$ be a kernel of a convolutional layer, where*

$$K_{(k,l,1,1)} = \begin{cases} 1 & \text{for } k = l, \\ 0 & \text{otherwise,} \end{cases} \quad k, l \in [3], \quad (9)$$

and Φ be a neural network with two convolutional layers with kernel K and one ReLU activation. The reduced network $\hat{\Phi}_\rho$, obtained by applying Thm. 1 using dynamic merge buckets, \mathcal{X} , and ρ , compresses the input \mathcal{X} with sound error bounds according to ρ .

Proof. The original network Φ computes the identity by construction. The image is compressed in the hidden layer of $\hat{\Phi}_\rho$ (Thm. 1). The computed bounds ensure $\mathcal{X} \subseteq \hat{\Phi}_\rho(\mathcal{X})$. \square

In the truck example in Fig. 4, for a perturbation radius $\epsilon = 0.01$ and a reduction rate $\rho = 0$, all 3072 neurons of the hidden layer of the compression network $\hat{\Phi}_\rho$ are dynamically merged using 21 merge buckets. Thus, the image is compressed into a 21-dimensional space in the hidden layer of $\hat{\Phi}_\rho$ and then re-enlarged to 3072 neurons in the output layer with added approximation error. Please note that usually, the image is not re-enlarged and the compressed image is passed to the next layer, where we again merge similar neurons using our approach – we just do this here for illustration purposes (Fig. 4): Due to the three color channels, the original truck image has 983 unique colors, which get compressed into 178 unique colors with formal error bounds. Similarly, the original horse image has 891 unique colors, which get compressed into 142 unique colors, again using 21 dynamic merge buckets.

In larger convolutional networks, a similar reduction happens in each hidden layer; however, these are usually not as easy to grasp visually due to the increased number of channels in hidden layers. Note that we can prepend the layers of the

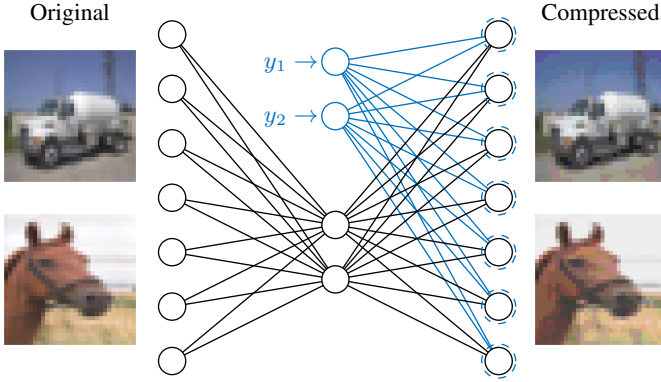


Fig. 4. Visualization of CIFAR-10 images: Original images (left) and corresponding compressed images (right), where we show all neurons within the same merge bucket $\mathcal{B}_{k,y_i,\delta} \in \mathcal{B}$ with value y_i without added approximation error. Verifying the compressed image with formal error bounds drastically reduces the number of neurons of hidden layers.

compression network defined in Cor. 1 to any network as a preprocessing step to reduce the input dimension.

The required steps for this preprocessing are provided in Alg. 3: We first construct the compression network as in Cor. 1. As we only compute the layers of the reduced network in line 2, we only require the input set represented as an interval \mathcal{X}_{int} . Thus, we can construct a new low-dimensional input \mathcal{H}_{-2} represented by the used set representation according to the remaining neurons. The output set is computed in line 5 by propagating the set through all remaining layers and reducing them on the fly (Alg. 2).

Algorithm 3 Sound Compression Preprocessing

Require: Input \mathcal{X}_{int} , neural network Φ_{org} , reduction rate ρ

- 1: $L_{-2}, L_{-1}, L_0 \leftarrow \text{Construct } \Phi_{\text{pre}}$ ▷ Cor. 1
- 2: $\widehat{L}_{-2}, \widehat{L}_{-1}, \widehat{L}_0 \leftarrow \text{Reduce } \Phi_{\text{pre}} \text{ using } \mathcal{X}_{\text{int}}, \rho$ ▷ Thm. 1
- 3: $\mathcal{H}_{-2} \leftarrow \langle \mathbf{0}, \square \rangle_{\mathcal{Z}} \oplus \widehat{L}_{-2}(\mathcal{X}_{\text{int}})$ ▷ Prop. 2
- 4: $\Phi'_{\text{org}}(\cdot) \leftarrow \Phi_{\text{org}}(\widehat{L}_0(\widehat{L}_{-1}(\cdot)))$ ▷ Prepend layers
- 5: $\mathcal{Y} \leftarrow \text{Execute Alg. 2 using } \mathcal{H}_{-2}, \Phi'_{\text{org}}, \rho$ ▷ Thm. 1
- 6: **return** \mathcal{Y}

Input sets are often given as an interval [7], and thus, we are not required to initialize the high-dimensional input set using a more complex set representation, i.e., a zonotope in our case. We only use the more complex set representation in the low-dimensional space and initialize it in line 3 with \mathcal{H}_{-2} . For zonotopes, this results in fewer generators as we create a new generator for each dimension in the respective interval (Prop. 2). Due to the on-the-fly reduction, the more complex set representation is kept in a low-dimensional space as by the time it arrives at a given layer, this layer is already reduced (Alg. 2). This becomes increasingly beneficial with the complexity of the set representation used to verify the network. Note that Alg. 3 works on any neural network, but is especially beneficial for convolutional networks because neighboring pixels often have similar values.

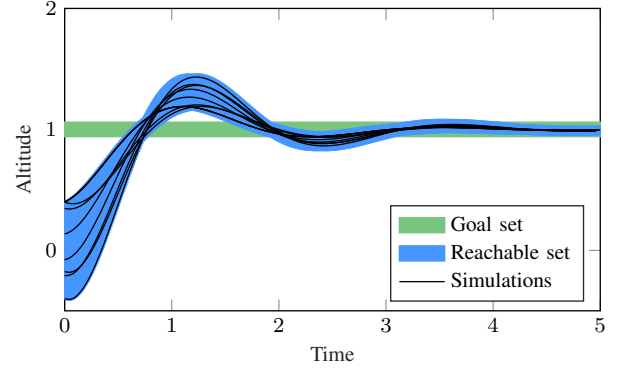


Fig. 5. Quadrotor example [9, Fig. 15]: As the reachable set stays within a given goal set, a reduced network can be reused as long as the reachable set stays within the goal set.

B. Reusing Reduced Networks

In general, our approach requires the computation of a new reduced neural network for different input sets. In this section, we highlight several applications where the reduced networks can be reused nevertheless:

1) *Branch-and-bound*: Current state-of-the-art tools, e.g., all top-ranked tools of the last VNN competition [8], verify a neural network by applying different kinds of branch-and-bound algorithms in the verification. Branch-and-bound algorithms [27] partition the verification problem into multiple simpler subproblems, solve them individually, and aggregate the results to reason about the overall problem. For example, splitting ReLU neurons into their linear parts [30] makes each subproblem simpler. This approach was later extended to other nonlinear functions [32].

Our novel reduction approach is orthogonal to these branch-and-bound algorithms and can be combined with them. Splitting a set usually requires more sophisticated set representations than zonotopes, as the splitted sets can, in general, no longer be represented by a zonotope. We can reuse the reduced network on all subsets of the input set since the reduced network does not depend on using a specific set representation:

Corollary 2 (Reusing Reduced Network on Subsets). *Given a neural network Φ , an input set \mathcal{X} , and a reduction rate ρ , then a reduced network $\widehat{\Phi}_\rho$ according to Thm. 1 can be reused for all $\mathcal{X}' \subseteq \mathcal{X}$.*

Proof. The proof follows from the construction of $\widehat{\Phi}_\rho$. □

2) *Closed-loop verification*: In closed-loop scenarios, a neural network is used as a controller in a dynamic system which is updated every Δt . While branch-and-bound strategies work well in open-loop verification, other techniques are more common in closed-loop scenarios [9]. The issue with branch-and-bound strategies is that each subset has to be propagated according to a differential equation until the next network evaluation, where each subset might again get splitted. Therefore, many techniques use more sophisticated set representation [18], [21], [22] and improve the abstraction by enclosing nonlinear functions with higher-order polynomials [23].

One frequent goal in closed-loop verification is to show the stability of a given dynamic system over a specified time horizon. For example, the QUAD benchmark in the last ARCH competition [9] requires showing the stability of a neural-network-controlled quadrotor at a given altitude (Fig. 5). We can infer from the simulations that the state of the system barely changes over the last second. Thus, we can slightly enlarge the current reachable set at $t = 4s$ and use it to reduce the size of the network. This reduced network can then be reused in subsequent evaluations if the reachable set stays within the set used to reduce the network controller (Cor. 2).

3) *Export of reduced network*: As the reduced network can be reused as described above, we provide an interface to export a reduced network for later usage, e.g., to verify the reduced network using another verification tool. Please note that a reduced network is of the form given in Def. 2, with the exception that the bias of a linear layer is an interval (Prop. 4). As biases can be seen as additional inputs to the network, most verifiers can verify networks of this form, including optimization-based verifiers.

V. EVALUATION

We evaluate our novel neural network reduction approach using several neural network variants and benchmarks from the VNN competition [7]. For all image datasets, we sample 100 correctly classified images from the test set and average the results. The perturbation radius $\epsilon \in \mathbb{R}_+$ is always stated with respect to the normalized images $\mathcal{X} \subset [0, 1]^{n_0}$. All following figures show the mean remaining input neurons per nonlinear layer $k \in [\kappa]$ as well as the number of input and output neurons of the network at 1 and $\kappa + 1$, respectively. We do not show the number of input neurons of linear layers, as a preceding nonlinear layer does not change the number of neurons. The number of neurons of the original network is shown in the same color with reduced opacity. Additionally, we show error bars indicating one standard deviation from the mean reduction per layer. If not otherwise stated, feed-forward neural networks are reduced using static merge buckets and convolutional neural networks using dynamic merge buckets (Sec. III-B).

We implemented our approach in MATLAB and use CORA [22], [53] to verify the neural networks. All computations were performed on an Intel® Core™ Gen. 11 i7-11800H CPU @2.30GHz with 64GB memory. We first show that our underlying assumption (Fig. 2) also holds in practice by choosing a fixed bucket tolerance δ , followed by automatically determining δ to obtain the desired network reduction ρ , where ρ is automatically increased if the image could not be verified.

A. Feed-Forward Neural Networks

1) *MNISTFC Benchmark*: In our first experiment, we used networks taken from the MNISTFC benchmark [7]. The benchmark uses images from the MNIST handwritten digit dataset. The images have a perturbation radius $\epsilon = 0.01$, and we use a bucket tolerance $\delta = 0.01$ for our evaluation. In Fig. 6, we show the reduction results on three neural networks with 6×256 , 4×256 , and 2×256 neurons. The reduced network retains, on average, only a small fraction of the neurons, ranging from

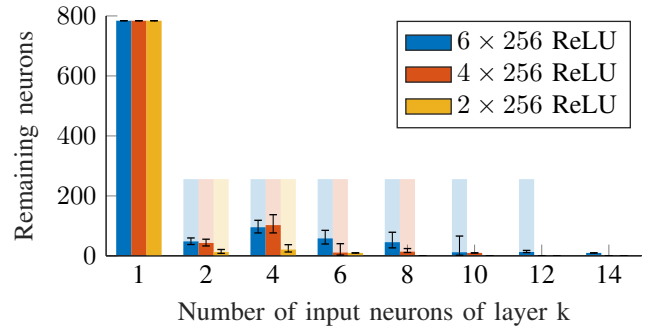


Fig. 6. MNISTFC benchmark: Networks with large reduction with static merge buckets. The error bars show one standard deviation from the mean reduction.

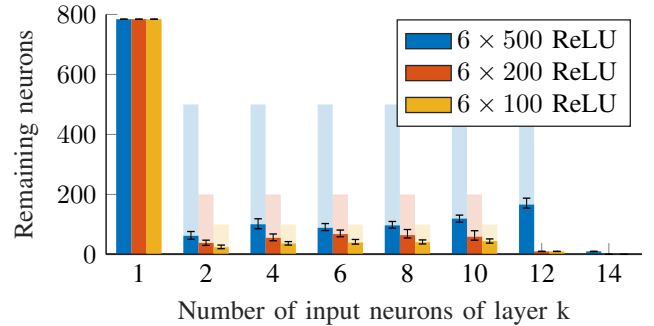


Fig. 7. ERAN network variants: We obtain similar formal reduction results compared to informal results in [41, Fig. 2 & Tab. 2].

5% to 15% depending on the size of the network. where more neurons remain in earlier layers and only a few in later layers. While our network reduction induces outer-approximation, we were still able to verify all images using the reduced networks.

2) *ERAN Benchmark*: The authors of [41] apply their reduction approach on multiple network variants of the ERAN benchmark¹. They first show that large informal network reductions using a small perturbation radius $\epsilon = 0.001$ are possible. However, once formal guarantees are demanded, 80 – 90% of the neurons remain [41, Fig. 2 & Tab. 2]. We obtained very similar reduction rates compared to their results; however, our approach provides sound error bounds: Fig. 7 shows the reduction results using a bucket tolerance $\delta = 0.005$ for the ReLU network of the ERAN benchmark and the two network variants with 6×100 , 6×200 , and 6×500 neurons, respectively. As we are able to reduce neural networks with any element-wise activation function using our approach, we can additionally reduce the network with sigmoid activations from the ERAN benchmark. Fig. 8 shows that we obtain similar reduction results using a bucket tolerance $\delta = 0.005$ for both networks.

Our approach automatically reduces neural networks by determining the bucket tolerance δ . However, how much the network is reduced for any given value for δ is not immediately clear. To illustrate how different values for δ affect the reduction results, Tab. I specifies the remaining number of neurons and the verification rate for varying perturbation radii ϵ and bucket

¹ Variants taken from the ERAN website: <https://github.com/eth-sri/eran>

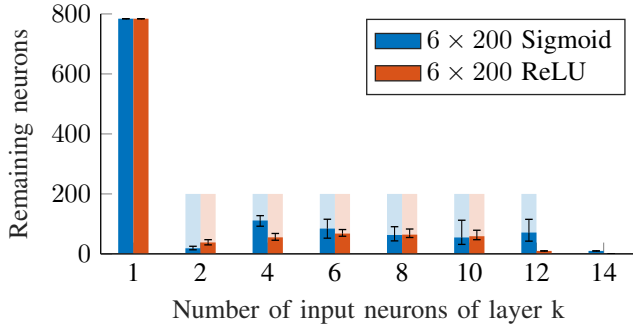


Fig. 8. ERAN benchmark: Networks with large reduction with static merge buckets for different activation functions.

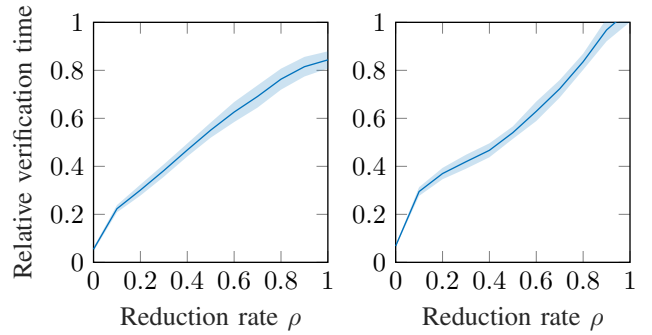


Fig. 9. The relative verification time of the reduced network primarily depends on the reduction rate ρ : ERAN sigmoid network (left) and ERAN CNN (right).

TABLE I
ERAN BENCHMARK: CHANGE OF VERIFICATION RATE (VR) AND REDUCTION RATE ρ WITH VARYING PERTURBATION RADIUS ϵ AND BUCKET TOLERANCE δ .

Network 6×200		Sigmoid		ReLU	
ϵ	δ	ρ	VR [%]	ρ	VR [%]
0.0050	0.1000	0.2392	69.00	0.5496	76.00
0.0050	0.0100	0.3700	99.00	0.5500	100.00
0.0050	0.0050	0.4242	100.00	0.5573	100.00
0.0050	0.0010	0.5146	100.00	0.5607	100.00
0.0050	0.0001	0.6380	100.00	0.5618	100.00
<hr/>					
0.0020	0.1000	0.1640	94.00	0.3602	95.00
0.0020	0.0100	0.3028	99.00	0.3556	100.00
0.0020	0.0050	0.3455	100.00	0.3549	100.00
0.0020	0.0010	0.4705	100.00	0.3479	100.00
0.0020	0.0001	0.6004	100.00	0.3494	100.00
<hr/>					
0.0010	0.1000	0.1318	98.00	0.3143	92.00
0.0010	0.0100	0.2782	100.00	0.2846	100.00
0.0010	0.0050	0.3336	100.00	0.2931	100.00
0.0010	0.0010	0.4507	100.00	0.2909	100.00
0.0010	0.0001	0.5882	100.00	0.2882	100.00

tolerances δ . The verification rate is the ratio of images that were verifiable with the reduced network compared to the original network. We iteratively reduce the bucket tolerance δ to measure how different merging strategies affect the reduction and verification: For the sigmoid network, a more aggressive merging strategy (large δ) results in fewer remaining neurons but yields a smaller total number of verified images. However, even for $\delta = 0.1$ over half of the images can be verified, and already more than 95% for the next smaller bucket tolerance. This tradeoff is less apparent for the ReLU network as most of the merged neurons in a nonlinear layer have an entirely negative input, thus, are merged regardless of the chosen bucket tolerance. The remaining variation is due to the neurons that have an input near 0. Note that a too aggressive merging strategy might lead to fewer remaining neurons in earlier layers, which can result in larger outer-approximation in later layers and thus fewer neurons being merged in total.

With these results, we apply our fully automatic approach from Sec. III-C to automatically determine the bucket tolerance δ to verify a given image. As the construction of the reduced network is computationally cheap, the verification time is reduced to a similar degree as shown in Fig. 9: We vary the desired reduction rate ρ and show the resulting average relative

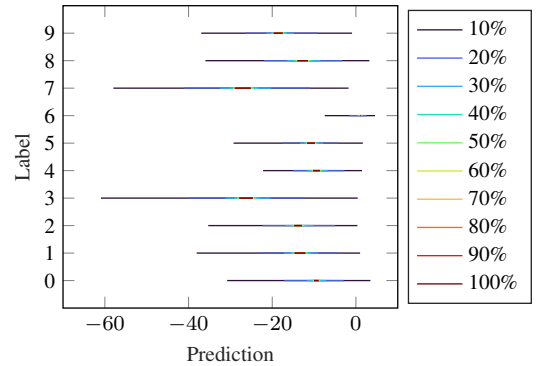


Fig. 10. Fully automatic network reduction: Comparison of outer-approximative bounds of the prediction for an MNIST image with $\epsilon = 0.01$ using the ERAN sigmoid network for different reduction rates ρ .

time to reduce and verify a network compared to verifying the original network directly. The average times to verify the original ERAN sigmoid network and the convolutional variant are $0.97s$ and $3.76s$, respectively. The surrounding region shows one standard deviation. Thus, we can verify most images using the reduced network for small ρ (Tab. I) in significantly less time (Fig. 9) and can iteratively increase ρ where the verification is more challenging. For a challenging MNIST image with label 6, Fig. 10 shows the computed outer-approximative output bounds using the ERAN sigmoid network for different ρ . The bounds quickly converge with increasing ρ , and the image can be verified with $\rho \geq 30\%$ in this example.

B. Convolutional Neural Networks

We demonstrate the unique advantage of our reduction approach on convolutional neural networks by explicitly exploiting similar neighboring pixels. The subsequent convolutional networks from ERAN are again trained on the MNIST handwritten image dataset, and the networks from the Marabou and Cifar2020 benchmarks are trained on the CIFAR-10 colored image dataset [7]. For all convolutional networks, we use dynamic merge buckets unless stated otherwise, normalize the input image, and repeat each experiment over 100 correctly classified images. To show that our underlying assumption of many pixels having similar colors holds in practice, we again first show the reduction results on the ERAN networks for a fixed bucket tolerance $\delta = \epsilon$. The results using our fully

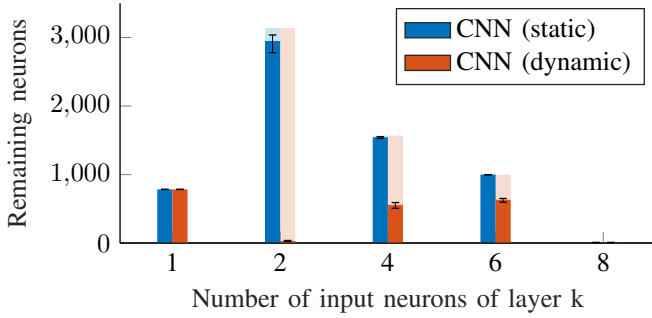


Fig. 11. Convolutional neural networks require dynamic merge buckets to exploit similar neighboring pixels.

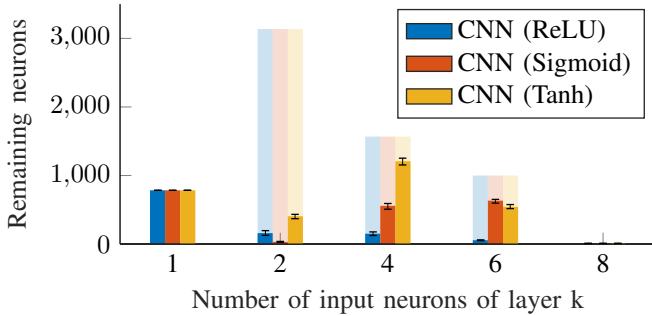


Fig. 12. ERAN networks with convolutional layers: Huge reductions are possible across all networks with different activation functions.

automatic reduction approach are then shown on the Marabou and Cifar2020 benchmarks.

1) *ERAN*: Fig. 11 shows the necessity for dynamic merge buckets to exploit similar neighboring pixels for a convolutional neural network with sigmoid activations. While barely any neurons are merged using static merge buckets, we obtain huge reductions using dynamic merge buckets, especially in the second layer, while still verifying the images. Further, we show a comparison of the reduction using networks with different activation functions in Fig. 12. Interestingly, large reductions can be achieved for all networks in the second layer. For the ReLU network, we can maintain a low number of neurons in later layers, too, while they increase again for the sigmoid and tanh networks for fixed δ . An equal reduction in all layers can be obtained using the fully automatic approach.

2) *Marabou*: We show the network reduction using our fully automatic approach on the Marabou benchmark in Fig. 13. The networks consist of two convolutional layers followed by three linear layers with ReLU activation. The input sets have a perturbation radius $\epsilon = 0.01$. Our fully automatic approach reduces these networks on average to $\sim 10\%$ of the original number of neurons. Please note that in layer 4, the remaining number of neurons are roughly equal for all three networks despite having different number of neurons in the original network.

3) *Cifar2020*: Next, we consider the networks from the Cifar2020 benchmark. This network is an order of magnitude larger than the other convolutional networks and is thus particularly hard to verify. The network consists of four convolutional layers with up to 32,768 neurons per layer

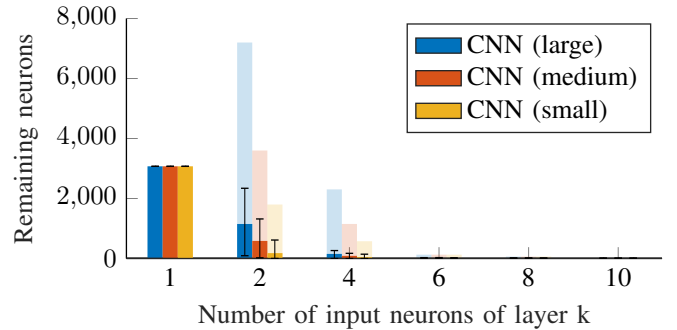


Fig. 13. Marabou benchmark: Fully automatic network reduction comparison of three networks on the CIFAR-10 dataset.

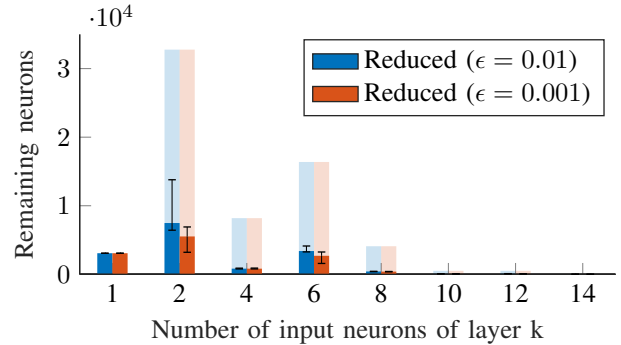


Fig. 14. Cifar2020 benchmark: Our fully automatic reduction approach is also applicable to very large networks.

followed by three linear layers and ReLU activation. We depict the reduction results of our network reduction in Fig. 14 for two different perturbation radii $\epsilon \in [0.01, 0.001]$. While the reduction results depend on the perturbation radius ϵ of the input set \mathcal{X} , the difference becomes less apparent in later layers.

4) *Compression network*: Fig. 15 shows how the sound compression preprocessing of the input image (Alg. 3) can further reduce the overall network size. The prepended layers shown at -1 and 0 only have very few remaining neurons, where we only show the number of neurons corresponding to the dimension of the constructed zonotope. Thus, the average total computation time is reduced from 4.59s to 0.78s as the initial reduction (Alg. 3, line 2) is computationally cheap and the representation of the involved sets is much smaller, i.e., the zonotopes have fewer generators, compared to verifying the original network. Our evaluation shows that, on average, only 28 input neurons remain for the ERAN CNN with sigmoid activation compared to the $28 \cdot 28 = 784$ input neurons of the original image (Fig. 15).

C. Reusing a Reduced Network

Finally, we give two examples where the reduced network was reused despite its input set restriction (Cor. 2).

1) *ACAS Xu benchmark*: We demonstrate the applicability of our approach on non-image data using the ACAS Xu benchmark [7]. The benchmark consists of multiple networks and properties used to verify turn advisories to an aircraft to avoid collisions. The networks have 6×50 hidden layers with

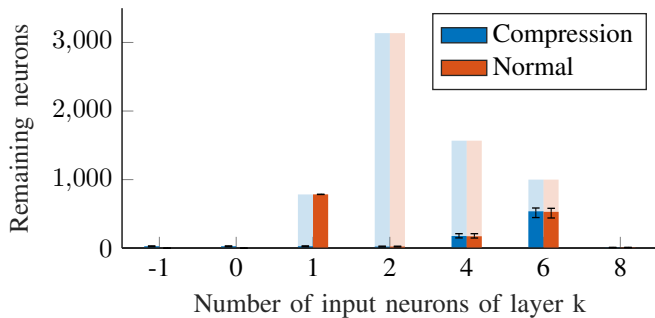


Fig. 15. ERAN CNN with sigmoid activation: Input compression (Alg. 3) versus normal reduction (Alg. 2).

TABLE II
AVERAGE NETWORK REDUCTION AND VERIFICATION TIME OF A PROPERTY OF THE ACAS XU BENCHMARK.

Neural Network	Number of Neurons	Verification Time
Original Network	100.00 %	7.38s
Reduced Network	61.33 %	4.21s

5 input and 5 output neurons. As this benchmark is particularly hard to verify, we apply a branch-and-bound strategy by recursively splitting the input set along the most sensitive dimension. Using Cor. 2, we can reduce the network once on the original input set and reuse the reduced network in all subsets. We show an example verification in Tab. II. The verification time also includes the time to reduce the network and is averaged over 10 runs. While the authors of [42] state that they can reduce the ACAS Xu networks down to a total number of 10 neurons, the obtained output sets are very conservative with a radius up to 10^{17} [42, Fig. 14-16], which makes it impossible to verify the given specifications.

2) *Closed-loop verification*: Finally, let us revisit the quadrotor example from Sec. IV-B to show the applicability of our approach in closed-loop systems: We enlarge the current reachable set at $t = 4s$ by a factor of 1.5 to compute the reduced network controller. This enlargement is necessary as the reachable set still oscillates around its equilibrium. The reduced network can then be reused in 60% of the remaining network evaluations. Whenever the current reachable set leaves the enlarged set used to reduce the network, the verification algorithm falls back to the original network until the reduced network can be used again. In the quadrotor example, the reduced network was always used again after one time step. Fig. 16 shows the relevant part of Fig. 5 and includes the reachable set computed with the reduced network, where both reachable sets remain within the desired goal region, and the reachable set computed with the reduced network is insignificantly larger.

VI. CONCLUSION

We present a fully automatic and sound neural network reduction approach, where the verification of the reduced network entails the verification of the original network. To the best of our knowledge, we present the first approach that works on all element-wise activation functions. The neural

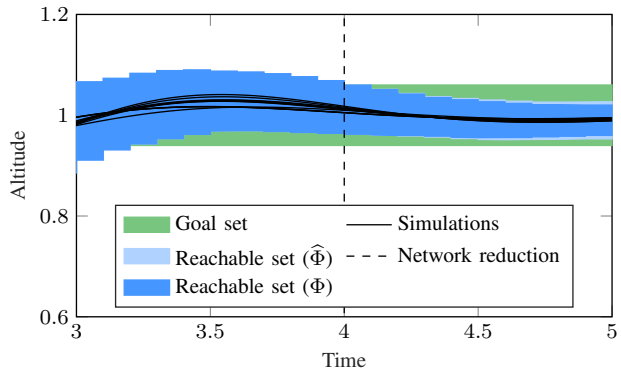


Fig. 16. Quadrotor example: We can reuse a reduced network $\hat{\Phi}$ once the system starts to converge to the desired altitude. The resulting reachable set is insignificantly larger.

network reduction is computed on the fly while verifying given specifications on the original network and merges neurons of nonlinear layers based on the output bounds of these neurons. The reduced network is computationally cheap to construct and does not induce large outer-approximations compared to the original network. All parameters of our approach are automatically tuned to minimize the network size without compromising verifiability and is orthogonal to many verification tools and thus can be combined with them. Further, our approach is the first to address the unique challenges of convolutional neural networks by explicitly exploiting similar neighboring pixels. Moreover, we show how our reduced network can be reused despite its restriction on the input set during branch-and-bound algorithms and closed-loop verification. Our evaluation shows the applicability of our approach on various benchmarks and network architectures, where the size of the networks is drastically reduced, which also decreases the total computation time.

ACKNOWLEDGEMENTS

The authors gratefully acknowledge financial support from the project FAI funded by the German Research Foundation (DFG) under project number 286525601. We also want to thank our colleagues Lukas Koller and Mark Wetzlinger from our research group for their revisions of the manuscript.

REFERENCES

- [1] A. B. Nassif, I. Shahin, I. Attili, M. Azzeh, and K. Shaalan, “Speech recognition using deep neural networks: A systematic review,” *IEEE access*, vol. 7, pp. 19 143–19 165, 2019.
- [2] Z. Li, F. Liu, W. Yang, S. Peng, and J. Zhou, “A survey of convolutional neural networks: Analysis, applications, and prospects,” *IEEE Transactions on Neural Networks and Learning Systems*, vol. 33, pp. 6999–7019, 2022.
- [3] D. Karimi and S. E. Salcudean, “Reducing the Hausdorff distance in medical image segmentation with convolutional neural networks,” *IEEE Transactions on Medical Imaging*, vol. 39, pp. 499–513, 2019.

- [4] D. Mukherjee, K. Gupta, L. H. Chang, and H. Najjaran, “A survey of robot learning strategies for human-robot collaboration in industrial settings,” *Robotics and Computer-Integrated Manufacturing*, vol. 73, 2022.
- [5] É. Zablocki, H. Ben-Younes, P. Pérez, and M. Cord, “Explainability of deep vision-based autonomous driving systems: Review and challenges,” *International Journal of Computer Vision*, vol. 130, pp. 2425–2452, 2022.
- [6] I. Goodfellow, J. Shlens, and C. Szegedy, “Explaining and harnessing adversarial examples,” in *International Conference on Learning Representations*, 2015.
- [7] S. Bak, C. Liu, and T. T. Johnson, “The second international verification of neural networks competition (VNN-COMP 2021): Summary and results,” *arXiv preprint arXiv:2109.00498*, 2021.
- [8] C. Brix, S. Bak, C. Liu, and T. T. Johnson, “The fourth international verification of neural networks competition (VNN-COMP 2023): Summary and results,” *arXiv preprint arXiv:2312.16760*, 2023.
- [9] D. M. Lopez, M. Althoff, M. Forets, T. T. Johnson, T. Ladner, and C. Schilling, “ARCH-COMP23 category report: Artificial intelligence and neural network control systems (AINNCS) for continuous and hybrid systems plants,” in *Proceedings of 10th International Workshop on Applied Verification for Continuous and Hybrid Systems*, vol. 96, 2023, pp. 89–125.
- [10] X. Huang, M. Kwiatkowska, S. Wang, and M. Wu, “Safety verification of deep neural networks,” in *International Conference on Computer Aided Verification*, 2017, pp. 3–29.
- [11] G. Katz, C. Barrett, D. L. Dill, K. Julian, and M. J. Kochenderfer, “Reluplex: An efficient SMT solver for verifying deep neural networks,” in *International Conference on Computer Aided Verification*, 2017, pp. 97–117.
- [12] H. Zhang, T.-W. Weng, P.-Y. Chen, C.-J. Hsieh, and L. Daniel, “Efficient neural network robustness certification with general activation functions,” *Advances in Neural Information Processing Systems*, vol. 31, 2018.
- [13] G. Katz, D. A. Huang, D. Ibeling, *et al.*, “The Marabou framework for verification and analysis of deep neural networks,” in *International Conference on Computer Aided Verification*, 2019, pp. 443–452.
- [14] M. N. Müller, G. Makarchuk, G. Singh, M. Püschel, and M. Vechev, “PRIMA: General and precise neural network certification via scalable convex hull approximations,” *Proceedings of the ACM on Programming Languages*, vol. 6, pp. 1–33, 2022.
- [15] T. Gehr, M. Mirman, D. Drachler-Cohen, P. Tsankov, S. Chaudhuri, and M. Vechev, “AI2: Safety and robustness certification of neural networks with abstract interpretation,” in *IEEE Symposium on Security and Privacy*, 2018, pp. 3–18.
- [16] G. Singh, T. Gehr, M. Mirman, M. Püschel, and M. Vechev, “Fast and effective robustness certification,” *Advances in Neural Information Processing Systems*, vol. 31, 2018.
- [17] R. Ivanov, T. Carpenter, J. Weimer, R. Alur, G. Pappas, and I. Lee, “Verisig 2.0: Verification of neural network controllers using Taylor model preconditioning,” in *International Conference on Computer Aided Verification*, 2021, pp. 249–262.
- [18] S. Bogomolov, M. Forets, G. Frehse, K. Potomkin, and C. Schilling, “JuliaReach: A toolbox for set-based reachability,” in *Proceedings of the 22nd ACM International Conference on Hybrid Systems: Computation and Control*, 2019, pp. 39–44.
- [19] C. Huang, J. Fan, X. Chen, W. Li, and Q. Zhu, “POLAR: A polynomial arithmetic framework for verifying neural-network controlled systems,” in *Automated Technology for Verification and Analysis*, 2022, pp. 414–430.
- [20] S. Bak, “nnenum: Verification of relu neural networks with optimized abstraction refinement,” in *NASA Formal Methods Symposium*, 2021, pp. 19–36.
- [21] D. M. Lopez, S. W. Choi, H.-D. Tran, and T. T. Johnson, “NNV 2.0: The neural network verification tool,” in *International Conference on Computer Aided Verification*, 2023, pp. 397–412.
- [22] N. Kochdumper, C. Schilling, M. Althoff, and S. Bak, “Open-and closed-loop neural network verification using polynomial zonotopes,” in *NASA Formal Methods Symposium*, 2023, pp. 16–36.
- [23] T. Ladner and M. Althoff, “Automatic abstraction refinement in neural network verification using sensitivity analysis,” in *Proceedings of the 26th ACM International Conference on Hybrid Systems: Computation and Control*, 2023, pp. 1–13.
- [24] P. Henriksen and A. Lomuscio, “Efficient neural network verification via adaptive refinement and adversarial search,” in *European Conference on Artificial Intelligence*, 2020, pp. 2513–2520.
- [25] G. Singh, T. Gehr, M. Püschel, and M. Vechev, “An abstract domain for certifying neural networks,” *Proceedings of the ACM on Programming Languages*, vol. 3, pp. 1–30, 2019.
- [26] C. Brix and T. Noll, “Debona: Decoupled boundary network analysis for tighter bounds and faster adversarial robustness proofs,” *arXiv preprint arXiv:2006.09040*, 2020.
- [27] R. Bunel, P. Mudigonda, I. Turkaslan, P. Torr, J. Lu, and P. Kohli, “Branch and bound for piecewise linear neural network verification,” *Journal of Machine Learning Research*, vol. 21, pp. 1–39, 2020.
- [28] E. Botoeva, P. Kouvaros, J. Kronqvist, A. Lomuscio, and R. Misener, “Efficient verification of relu-based neural networks via dependency analysis,” in *Proceedings of the AAAI Conference on Artificial Intelligence*, vol. 34, 2020, pp. 3291–3299.
- [29] G. Singh, T. Gehr, M. Püschel, and M. Vechev, “Boosting robustness certification of neural networks,” in *International Conference on Learning Representations*, 2018.
- [30] S. Wang, H. Zhang, K. Xu, *et al.*, “Beta-CROWN: Efficient bound propagation with per-neuron split constraints for complete and incomplete neural network verification,” *Advances in Neural Information Processing Systems*, vol. 34, 2021.

- [31] C. Ferrari, M. N. Mueller, N. Jovanović, and M. Vechev, “Complete verification via multi-neuron relaxation guided branch-and-bound,” in *International Conference on Learning Representations*, 2022.
- [32] Z. Shi, Q. Jin, J. Z. Kolter, S. Jana, C.-J. Hsieh, and H. Zhang, “Formal verification for neural networks with general nonlinearities via branch-and-bound,” *2nd Workshop on Formal Verification of Machine Learning*, 2023.
- [33] L. Pulina and A. Tacchella, “An abstraction-refinement approach to verification of artificial neural networks,” in *International Conference on Computer Aided Verification*, 2010, pp. 243–257.
- [34] W. Xiang, H.-D. Tran, and T. T. Johnson, “Output reachable set estimation and verification for multilayer neural networks,” *IEEE Transactions on Neural Networks and Learning Systems*, vol. 29, pp. 5777–5783, 2018.
- [35] A.-K. Kopetzki and S. Günemann, “Reachable sets of classifiers and regression models: (Non-)robustness analysis and robust training,” *Machine Learning*, vol. 110, pp. 1175–1197, 2021.
- [36] K. Makino and M. Berz, “Taylor models and other validated functional inclusion methods,” *International Journal of Pure and Applied Mathematics*, vol. 6, pp. 239–316, 2003.
- [37] S. Bak and P. S. Duggirala, “Simulation-equivalent reachability of large linear systems with inputs,” in *International Conference on Computer Aided Verification*, 2017, pp. 401–420.
- [38] N. Kochdumper and M. Althoff, “Sparse polynomial zonotopes: A novel set representation for reachability analysis,” *IEEE Transactions on Automatic Control*, vol. 66, pp. 4043–4058, 2020.
- [39] Y. Y. Elboher, J. Gottschlich, and G. Katz, “An abstraction-based framework for neural network verification,” in *International Conference on Computer Aided Verification*, 2020, pp. 43–65.
- [40] P. Prabhakar and Z. R. Afzal, “Abstraction based output range analysis for neural networks,” *Advances in Neural Information Processing Systems*, vol. 32, 2019.
- [41] P. Ashok, V. Hashemi, J. Křetínský, and S. Mohr, “DeepAbstract: Neural network abstraction for accelerating verification,” in *International Symposium on Automated Technology for Verification and Analysis*, 2020, pp. 92–107.
- [42] F. Boudardara, A. Boussif, P.-J. Meyer, and M. Ghazel, “INNAbstract: An INN-based abstraction method for large-scale neural network verification,” *IEEE Transactions on Neural Networks and Learning Systems*, 2023.
- [43] B. Neyshabur, Z. Li, S. Bhojanapalli, Y. LeCun, and N. Srebro, “Towards understanding the role of over-parametrization in generalization of neural networks,” *arXiv preprint arXiv:1805.12076*, 2018.
- [44] L. Zhangheng, T. Chen, L. Li, B. Li, and Z. Wang, “Can pruning improve certified robustness of neural networks?” *Transactions on Machine Learning Research*, 2022.
- [45] L. Deng, G. Li, S. Han, L. Shi, and Y. Xie, “Model compression and hardware acceleration for neural networks: A comprehensive survey,” *Proceedings of the IEEE*, vol. 108, pp. 485–532, 2020.
- [46] J. Cheng, J. Wu, C. Leng, Y. Wang, and Q. Hu, “Quantized CNN: A unified approach to accelerate and compress convolutional networks,” *IEEE Transactions on Neural Networks and Learning Systems*, vol. 29, pp. 4730–4743, 2017.
- [47] L. Gonzalez-Carabarin, I. A. Huijben, B. Veeling, A. Schmid, and R. J. van Sloun, “Dynamic probabilistic pruning: A general framework for hardware-constrained pruning at different granularities,” *IEEE Transactions on Neural Networks and Learning Systems*, vol. 35, pp. 733–744, 2024.
- [48] M. Sotoudeh and A. V. Thakur, “Abstract neural networks,” in *Static Analysis*, 2020, pp. 65–88.
- [49] F. Boudardara, A. Boussif, P.-J. Meyer, and M. Ghazel, “Interval weight-based abstraction for neural network verification,” in *International Conference on Computer Safety, Reliability, and Security*, 2022, pp. 330–342.
- [50] Y. Y. Elboher, E. Cohen, and G. Katz, “Neural network verification using residual reasoning,” in *International Conference on Software Engineering and Formal Methods*, 2022, pp. 173–189.
- [51] Y. Zhong, R. Wang, and S.-C. Khoo, “Expediting neural network verification via network reduction,” *arXiv preprint arXiv:2308.03330*, 2023.
- [52] A. Girard, “Reachability of uncertain linear systems using zonotopes,” in *International Workshop on Hybrid Systems: Computation and Control*, 2005, pp. 291–305.
- [53] M. Althoff, “An introduction to CORA 2015,” in *Proc. of the Workshop on Applied Verification for Continuous and Hybrid Systems*, 2015, pp. 120–151.
- [54] C. M. Bishop and N. M. Nasrabadi, *Pattern recognition and machine learning*. 2006, vol. 4.
- [55] M. Althoff, “Reachability analysis and its application to the safety assessment of autonomous cars,” Ph.D. dissertation, Technische Universität München, 2010.
- [56] A. Rakitianskaia and A. Engelbrecht, “Measuring saturation in neural networks,” in *IEEE Symposium Series on Computational Intelligence*, 2015, pp. 1423–1430.
- [57] A. Bäuerle, D. Jönsson, and T. Ropinski, “Neural activation patterns (NAPs): Visual explainability of learned concepts,” *arXiv preprint arXiv:2206.10611*, 2022.
- [58] L. Jaulin, M. Kieffer, O. Didrit, and É. Walter, *Interval analysis*. 2001.